Received: 17 October 2023 | Revised: 16 January 2024 | Accepted: 5 February 2024

DOI: 10.1002/aoc.7408

FULL PAPER

Applied Organometallic Chemistry WILEY

Synthesis, characterization, and photocatalytic activity for water remediation and hydrogen evolution of Zn(II) and Ni(II) bis(thiosemicarbazone) complexes

Rodrigo Burón[1] | **Daniel Jiménez-Gómez**[2] | **David G. Calatayud**[1] | **Ana Iglesias-Juez**[2] | **Fernando Fresno**[2] | **M. Antonia Mendiola**[1] | **Elena López-Torres**[1]

[1]Departamento de Química Inorgánica, Universidad Autónoma de Madrid, Madrid, Spain

[2]Instituto de Catálisis y Petroleoquímica, CSIC, Madrid, Spain

Correspondence
David G. Calatayud and Elena López-Torres, Departamento de Química Inorgánica, Universidad Autónoma de Madrid, Cantoblanco, 28049 Madrid, Spain.
Email: david.gcalatayud@uam.es and elena.lopez@uam.es

Funding information
Ministerio de Ciencia e Innovación, Grant/Award Number: PID2019-104118RB-C21

The extensive industrial use of organic dyes causes large amounts of these substances to arrive at water sources, so nowadays, organic compound removal from fresh water is a major concern. The use of photocatalysts is an interesting approach to solving this problem, with coordination compounds playing an outstanding role. We report the selective synthesis and characterization of three new dissymmetric bis(thiosemicarbazone) ligands and their nickel(II) and zinc(II) complexes, which have been fully characterized by several techniques. The photocatalytic activity of the six complexes for methyl orange degradation was also evaluated. All the complexes can degrade this organic dye, although the photoefficiency of the nickel compounds is, in general, higher than for the zinc ones, as the degradation is faster and they do not reach a plateau. Density functional theory calculations show a clear dependence of the highest occupied molecular orbital (HOMO)–lowest unoccupied molecular orbital (LUMO) gap, as well as with the relative energies of these orbitals. On the other hand, the need for green fuels that do not produce the greenhouse effect is one of the major goals of modern life, and molecular hydrogen is one of the most promising ones. Considering the proven potential of bis(thiosemicarbazone) complexes to electrocatalyze H_2 evolution recently reported in the literature, we also made some preliminary tests to investigate the potential of the nickel complexes to act as photocatalysts for water splitting. The results indicate that two of the complexes produce H_2 in the conditions tested, so they could be used in the development of efficient photocatalytic systems for hydrogen evolution.

KEYWORDS
bis(thiosemicarbazones), nickel complexes, photocatalysis, water remediation, zinc complexes

1 | INTRODUCTION

Due to their extensive use in many types of industries, one of the most widespread water contaminants are organic dyes, which are reported to be responsible for respiratory toxicity and cancer.[1,2] Currently, the approaches to dye removal mainly depend on traditional biological, physical, and chemical techniques, such as precipitation, coagulation, adsorption, filtration, membrane separation, or biodegradation, but they are far from satisfactory, mainly due to cost control and harmless processing.[3–6] To solve this problem, different photocatalytic approaches are being developed to remove pollutants from wastewater, due to their potential to degrade and mineralize toxic organic dyes into less harmful compounds such as H_2O, CO_2, and NO_3^-.[7–9] Among the different possible photocatalysts, transition metal-based coordination compounds have given rise to diverse and flexible ways of promoting photocatalytic efficiency.[10–12]

Thiosemicarbazones (TSCs) are strong chelating ligands for transition metal ions that have received considerable attention because they exhibit a wide range of interesting properties mainly related to pharmacological applications, among others, antitumor,[13] antioxidant,[14] and antimicrobial activity,[15] and hypoxic selectivity.[16] Nevertheless, the potential of TSC complexes to catalyze different reactions has been sparingly investigated and is almost restricted to different organic reactions such as alkylations or coupling reactions.[17,18]

Within TSC, bis(thiosemicarbazones) show improved features as they form more stable coordination compounds due to their higher denticity and the formation of more chelate rings.[19] In addition, dissymmetric bis(thiosemicarbazones) can be even more interesting, as different functional groups, contributing different electronic and structural properties, can be incorporated into the ligands and their resulting complexes.[20] Unfortunately, the synthesis of this type of ligand is not straightforward, as two successive condensation reactions are required, increasing the possibility of obtaining undesired by-products resulting, for example, from double condensation or cyclization.[21] For the last few years, our group has been working on the design and synthesis of unsymmetrical ligands incorporating TSC moieties and has developed several synthetic approaches to selectively obtain this type of ligand with high purity and yield.[22–26]

In this paper, we report the synthesis and characterization of three new dissymmetric bis(thiosemicarbazone) ligands and their nickel(II) and zinc(II) complexes. We have explored their potential to be used as photocatalysts for methyl orange (MO) degradation. Density functional theory (DFT) calculations, which have been proven to provide relevant information about reactivity trends and different properties of the complexes,[27] were used in order to explain the results obtained. Recently, the use of bis(thiosemicarbazone) complexes as electrocatalysts in hydrogen evolution reactions (HERs) was described and attributed to their own redox activity together with the existence of different protonation sites (sulfur and nitrogen atoms) that allow these ligands to act as proton relays.[28,29] Based on these interesting results, we also made some preliminary assays to test the photoactivity of the nickel complexes for water splitting reactions.

2 | EXPERIMENTAL

All the products and solvents were obtained from standard commercial sources and used without further purification. Microanalyses were carried out using a LECO CHNS-932 elemental analyzer. Infrared (IR) spectra were obtained from KBr pellets on a Jasco FT/IR-410 spectrophotometer in the 4000–325 cm^{-1} range. The electrospray ionization (ESI) mass spectra in positive mode were recorded on a Q-STAR PULSAR I instrument using a hybrid analyzer, QTOF (quadrupole time-of-flight). ^1H and ^{13}C nuclear magnetic resonance (NMR) spectra were recorded on a Bruker AVIII HD spectrophotometer with dimethyl sulfoxide (DMSO)-d_6 as solvent and tetramethylsilane (TMS) as reference. UV–vis spectra were acquired on an ATi Unicam UV2 spectrophotometer using freshly prepared DMSO solutions.

2.1 | Synthesis of the organic compounds

2.1.1 | 4-(1-Naphthyl)-3-thiosemicarbazide (NfTs)

It was synthetized following the previously reported procedure.[30]

2.1.2 | 4-(4-Chlorophenyl)-3-thiosemicarbazide (ClPhTs)

To a solution of 2.000 g (11.8 mmol) of 4-chlorophenyl isothiocyanate in 50 mL of diethyl ether was added 0.7 mL (14.0 mmol) of hydrazine monohydrate, and the mixture was stirred at room temperature for 1 h. The white solid formed was filtered, thoroughly washed with diethyl ether, and dried in vacuum, obtaining 2.209 g (93% yield). ^1H NMR (300 MHz, DMSO-d_6) δ (ppm): 9.22 (s, 2H, $H_5 + H_6$), 7.71 (d, $J = 8.6$ Hz, 2H, $H_1 + H_4$), 7.35 (d, $J = 8.8$ Hz, 2H, $H_2 + H_3$), 4.89 (s, 2H, H_{7a}).

2.1.3 | 4-(4-Methoxyphenyl)-3-thiosemicarbazide (OMePhTs)

Six milliliters (11.9 mmol) of hydrazine monohydrate was added to a solution containing 1.3 mL (9.4 mmol) of 4-methoxyphenyl isothiocyanate, and the mixture was stirred for 1 h at room temperature. The white solid formed was filtered, thoroughly washed with diethyl ether, and dried in vacuum, obtaining 1.702 g (92% yield). ^{1}H NMR (300 MHz, DMSO-d_6) δ (ppm): 9.50 (b s, 1H, H_5), 8.97 (s, 1H, H_6), 7.45 (d, $J = 8.9$ Hz, 1H, $H_1 + H_4$), 6.88 (d, $J = 9.0$ Hz, 2H, $H_2 + H_3$), 4.83 (b s, 2H, H_{7a}), 3.74 (s, 3H, H_{3a}).

2.1.4 | Diacetyl-2-thiosemicarbazone (HATs)

The compound was obtained following the procedure previously described.[31] ν_{max} (cm^{-1}): 3399, 3326, and 3182 (NH), 1685 (CO), 1587 (NH_2), 852 (thioamide IV). δH (300 MHz, DMSO-d_6, Me_4Si) 10.58 (1H, s, NH), 8.71 (1H, s, NH_2), 8.10 (1H, s, NH_2), 2.40 (3H, s, CH_3CO), 1.97 (3H, s, CH_3CN).

2.1.5 | Diacetyl-2-(thiosemicarbazone)-3-(1-naphthyl-3-thiosemicarbazone) ($\mathbf{L^1H_2}$)

A suspension of 0.500 g (1.7 mmol) of HATs in 6 mL of ethanol with three drops of hydrochloric acid was mixed with a suspension of 0.682 g (1.7 mmol) of 4-(1-naphthyl)-3-thiosemicarbazide in 4 mL of ethanol with one drop of hydrochloric acid. The mixture was stirred at room temperature for 24 h, and the yellow solid was filtered, washed with ethanol, and vacuum dried. (84% yield). Anal. calcd. for $C_{16}H_{18}N_6S_2$ (molecular weight [MW] 358.45) (%): C, 53.61; H, 5.06; N, 23.44; S, 17.89. Found (%): C, 53.87; H, 5.14; N, 23.15; S, 17.93. Mass spectrometry (MS) m/z: 358.11 $[M + H]^+$, 717.21 $[2M + H]^+$. IR (KBr) ν (cm^{-1}): 3437, 3328, 3239, 3157 (NH), 1597 (C═N), 1495, 1463 (HNH, thioamide I, CC_{ar}), 834 (thioamide IV), 770 (CH_{oop}). ^{1}H NMR (300 MHz, DMSO-d_6) δ (ppm): 10.70 (s, 1H, H_{5a}), 10.24 (s, 1H, H_{6a}), 10.23 (s, 1H, H_2), 8.44 (s, 1H, H_{1a}), 8.02–7.96 (m, 1H, H_{16}), 7.94–7.89 (m, 2H, $H_{13} + H_{1b}$), 7.86–7.83 (m, 1H, H_{10}), 7.60–7.52 (m, 4H, $H_{15} + H_{14} + H_9 + H_8$), 2.31, 2.29 (s, 3H; s, 3H; H_5, H_6). ^{13}C NMR (75 MHz, DMSO-d_6) δ (ppm): 179.4 (C_1), 179.2 (C_4), 149.7 (C_2), 146.9 (C_3), 136.1 (C_7), 134.2 (C_{11}), 130.8 (C_{16}), 128.6 (C_9), 127.4 (C_{15}), 126.7 (C_{14}), 126.6 (C_{12}), 126.5 (C_{13}), 125.9 (C_{10}), 123.6 (C_8), 12.4, 12.3 (C_5, C_6).

2.1.6 | Diacetyl-2-(thiosemicarbazone)-3-(4-chlorophenyl-3-thiosemicarbazone) ($\mathbf{L^2H_2}$)

It was synthesized following the same procedure described for the synthesis of $\mathbf{L^1H_2}$ but adding 0.633 g (1.7 mmol) of 4-(4-chlorophenyl)-3-thiosemicarbazide. (86% yield). Anal. calcd. for $C_{12}H_{15}N_6S_2Cl$ (MW 342.83) (%): C, 42.04; H, 4.41; N, 24.51; S, 18.70. Found (%): C, 42.35; H, 4.68; N, 22.98; S, 18.62. MS m/z: 343.06 $[M + H]^+$. IR (KBr) ν (cm^{-1}): 3409, 3303, 3209, 3149 (NH), 1598 (C═N), 1527, 1503, 1492 (HNH, thioamide I, CC_{ar}), 849 (thioamide IV), 832, 796 (CH_{oop}). ^{1}H NMR (300 MHz, DMSO-d_6) δ (ppm): 10.69 (s, 1H, H_{6a}), 10.27 (s, 1H, H_2), 9.98 (s, 1H, H_{5a}), 8.44 (s, 1H, H_{1a}), 7.89 (s, 1H, H_{1b}), 7.62 (d, $J = 8.8$ Hz, 2H, $H_8 + H_{12}$), 7.43 (d, $J = 8.8$ Hz, 2H, $H_9 + H_{11}$), 2.26 (s, 6H, $H_5 + H_6$). ^{13}C NMR (75 MHz, DMSO-d_6) δ (ppm): 179.4 (C_1), 177.4 (C_4), 150.1 (C_2), 148.6 (C_3), 138.5 (C_7), 129.9 (C_{10}), 128.5 ($C_9 + C_{11}$), 127.7 ($C_8 + C_{12}$), 12.4, 12.3 (C_5, C_6).

2.1.7 | Diacetyl-2-(thiosemicarbazone)-3-(4-methoxyphenyl-3-thiosemicarbazone) ($\mathbf{L^3H_2}$)

It was synthesized following the same procedure described for the synthesis of $\mathbf{L^1H_2}$ but adding 0.619 g (1.7 mmol) of 4-(4-methoxyphenyl)-3-thiosemicarbazide. (89% yield). Anal. calcd. for $C_{13}H_{18}N_6S_2O$ (MW 338.42) (%): C, 46.13; H, 5.36; N, 24.83; S, 18.95. Found (%): C, 46.34; H, 5.54; N, 24.68; S, 18.73. MS m/z: 339.11 $[M + H]^+$, 361.09 $[M + Na]^+$. IR (KBr) ν (cm^{-1}): 3413, 3339, 3310, 3236, 3157 (N—H), 1600 (C═N), 1534, 1521, 1494 (HNH, thioamide I, CC_{ar}), 847 (thioamide IV), 829, 810 (CH_{oop}). ^{1}H NMR (300 MHz, DMSO-d_6) δ (ppm): 10.49 (s, 1H, H_{6a}), 10.24 (s, 1H, H_2), 9.84 (s, 1H, H_{5a}), 8.42 (s, 1H, H_{1a}), 7.88 (s, 1H, H_{1b}), 7.41 (d, $J = 9.0$ Hz, 2H, $H_8 + H_{12}$), 6.94 (d, $J = 9.0$ Hz, 2H, $H_9 + H_{11}$), 3.77 (s, 3H, H_{13}), 2.25 (s, 3H, H_6), 2.24 (s, 3H, H_5). ^{13}C NMR (75 MHz, DMSO-d_6) δ (ppm): 179.4 (C_1), 177.7 (C_4), 157.5 (C_{10}), 149.4 (C_3), 148.7 (C_4), 132.4 (C_7), 127.8 ($C_9 + C_{11}$), 113.8 ($C_8 + C_{12}$), 55.7 (C_{13}), 12.3, 12.2 (C_5, C_6).

2.2 | Synthesis of the coordination compounds

The six complexes were synthesized following the same procedure, in which a solution of 0.27 mmol of $Ni(NO_3)_2{\cdot}6H_2O$ or 0.32 mmol of $Zn(NO_3)_2{\cdot}6H_2O$ with 0.64 mmol of $LiOH{\cdot}H_2O$ in 1 mL of ethanol was added to

a suspension containing 0.27 mmol of the corresponding ligand and 5 mL of the same solvent. The mixture was refluxed for 2 h, and the resulting solid was filtered, washed with water and ethanol, and dried on filter paper.

2.2.1 | [NiL^1] (**1**)

Brown, 108 mg, 93%. Anal. calcd. for $NiC_{16}H_{16}N_6S_2$ (MW 415.16) (%): C, 46.29; H, 3.88; N, 20.24; S, 15.44. Found (%): C, 46.00; H, 3.89; N, 19.52; S, 15.38. ESI-MS m/z: 415.03 $[M + H]^+$, 829.05 $[2M + H]^+$. IR (KBr) ν (cm^{-1}): 3348, 3311, 3204 (NH), 1598, 1584 (C═N), 1535, 1489, 1439 (thioamide I + H—N—H, CC_{ar}), 852 (thioamide IV), 790, 765 (CH_{oop}), 440, 435 (Ni—N), 334, 331 (Ni—S). ^{1}H NMR (300 MHz, DMSO-d_6) δ (ppm): 9.95 (s, 1H, H_{6a}), 7.98–7.89 (m, 2H, $H_{13} + H_{16}$), 7.78 (d, $J = 9.5$ Hz, 1H, H_{10}), 7.59–7.45 (m, 6H, $H_8 + H_9 + H_{14} + H_{15} + H_{1a} + H_{1b}$), 1.88 (s, 3H, H_5), 1.81 (s, 3H, H_6). ^{13}C NMR (75 MHz, DMSO-d_6) δ (ppm): 179.5, 177.4 (C_1, C_4), 158.2, 154.7 (C_2, C_3), 136.3 (C_7), 134.0 (C_{11}), 129.0 (C_{16}), 128.4 (C_9), 126.6 (C_{15}), 126.4 (C_{14}), 126.3 (C_{12}), 125.8 (C_{13}), 124.0 (C_{10}), 123.58 (C_8), 14.5 (C_5), 14.2 (C_6). UV–vis (DMSO) λ_{max} nm (L mol^{-1} cm^{-1}): 268 (25,180), 414 (12,790), 680 (596).

2.2.2 | [ZnL^1(OH$_2$)] (**2**)

Yellow, 117 mg, 95%. Anal. calcd. for $ZnC_{16}H_{18}N_6S_2O$ (MW 439.86) (%): C, 43.69; H, 4.12; N, 19.11; S, 14.58. Found (%): C, 43.45; H, 3.99; N, 19.22; S, 14.36. ESI-MS m/z: 211.02 $[ZnL^1 + H]^{2+}$, 421.02 $[ZnL^1 + H]^+$, 845.04 $[Zn_2(L^1)_2 + H]^+$, 1265.05 $[Zn_3(L^1)_3 + H]^+$. IR (KBr) ν (cm^{-1}): 3448, 3360, 3292, 3176 (O—H + N—H), 1636, 1595, 1582 (HOH + C═N), 1535, 1491, 1454, 1431 (thioamide I + HNH, CC_{ar}), 845 (thioamide IV), 791, 758 (CH_{oop}), 421, 418 (Zn—N), 350, 338 (Zn—S). ^{1}H NMR (300 MHz, DMSO-d_6) δ (ppm): 9.25 (s, 1H, H_{6a}), 8.05–7.99 (m, 1H, H_{16}), 7.93–7.87 (m, 1H, H_{13}), 7.73–7.67 (m, 2H, $H_{10} + H_{13}$), 7.54–7.45 (m, 3H, $H_8 + H_9 + H_{14}$), 7.00 (s, 2H, $H_{1a} + H_{1b}$), 2.16 (s, 3H, H_5), 2.05 (s, 3H, H_6). ^{13}C NMR (75 MHz, DMSO-d_6) δ (ppm): 179.1, 176.2 (C_1, C_4), 148.2, 144.1 (C_2, C_3), 136.5 (C_7), 134.2 (C_{11}), 129.2 (C_{16}), 128.3 (C_9), 126.2 (C_{15}), 125.9 (C_{14}), 125.8 (C_{12}), 125.0 (C_{13}), 124.1 (C_{10}), 123.4 (C_8), 14.6 (C_5), 14.3 (C_6). UV–vis (DMSO) λ_{max} nm (L mol^{-1} cm^{-1}): 264 (18,530), 330 (17,110), 450 (16,840).

2.2.3 | [NiL^2] (**3**)

Brown, 120 mg, 95%. Anal. calcd. for $NiC_{12}H_{13}N_6S_2Cl$ (MW 399.54) (%): C, 36.07; H, 3.28; N, 21.03; S, 16.05. Found (%): C, 35.74; H, 3.13; N, 21.32; S, 15.83. ESI-MS m/z: 397.97 $[M + H]^+$, 796.94 $[2M + H]^+$. IR (KBr) ν (cm^{-1}): 3376, 3265, 3182, 3155 (N—H), 1605 (C═N), 1546, 1492 (thioamide I + HNH, CC_{ar}), 865 (thioamide IV), 825 (CH_{oop}), 449, 428 (Ni—N), 347, 338 (Ni—S). ^{1}H NMR (300 MHz, DMSO-d_6) δ (ppm): 9.96 (s, 1H, H_{6a}), 7.66 (b s, 2H, $H_{1a} + H_{1b}$), 7.61 (d, $J = 9.0$ Hz, 2H, $H_8 + H_{12}$), 7.33 (d, $J = 9.0$ Hz, 2H, $H_9 + H_{11}$), 2.05 (s, 3H, H_6), 1.93 (s, 3H, H_5). ^{13}C NMR (75 MHz, DMSO-d_6) δ (ppm): 179.8, 172.9 (C_1, C_4), 160.8, 154.5 (C_2, C_3), 139.8 (C_7), 128.9 (C_{10}), 126.7 ($C_9 + C_{11}$), 121.5 ($C_8 + C_{12}$), 15.2, 14.3 (C_5, C_6). UV–vis (DMSO) λ_{max} nm (L mol^{-1} cm^{-1}): 270 (37,280), 425 (21,850), 677 (611).

2.2.4 | [ZnL^2(OH$_2$)] (**4**)

Brown, 127 mg, 90%. Anal. calcd. for $ZnC_{12}H_{15}N_6S_2OCl$ (MW 424.24) (%): C, 33.97; H, 3.56; N, 19.81; S, 15.11. Found (%): C, 33.61; H, 3.39; N, 20.14; S, 14.88. ESI-MS m/z: 404.97 $[ZnL^2 + H]^+$, 808.93 $[Zn_2(L^2)_2 + H]^+$, 1212.89 $[Zn_3(L^2)_3 + H]^+$. IR (KBr) ν (cm^{-1}): 3478, 3263, 3168, 3107 (OH + NH), 1613, 1592 (HOH + C═N), 1537, 1487, 1453 (thioamide I + HNH + CC_{ar}), 858 (thioamide IV), 818 (CH_{oop}), 442, 420 (Zn—N), 339, 328 (Zn—S). ^{1}H NMR (300 MHz, DMSO-d_6) δ (ppm): 9.47 (s, 1H, H_{6a}), 7.84 (d, $J = 9.0$ Hz, 2H, $H_8 + H_{12}$), 7.30 (d, $J = 9.0$ Hz, 2H, $H_9 + H_{11}$), 7.11 (s, 2H, $H_{1a} + H_{1b}$), 2.30 (s, 3H, H_6), 2.22 (s, 3H, H_5). ^{13}C NMR (75 MHz, DMSO-d_6) δ (ppm): 179.4, 172.9 (C_1, C_4), 150.2, 143.8 (C_2, C_3), 140.6 (C_7), 128.6 (C_{10}), 125.2 ($C_9 + C_{11}$), 121.7 ($C_8 + C_{12}$), 15.3, 14.4 (C_5, C_6). UV–vis (DMSO) λ_{max} nm (L mol^{-1} cm^{-1}): 258 (12,760), 332 (13,300), 445 (14,300).

2.2.5 | [NiL^3] (**5**)

Brown, 119 mg, 94%. Anal. calcd. for $NiC_{13}H_{16}N_6S_2O$ (MW 395.13) (%): C, 39.52; H, 4.02; N, 21.27; S, 16.23. Found (%): C, 39.33; H, 3.87; N, 21.46; S, 16.11. ESI-MS m/z: 395.03 $[M + H]^+$, 789.04 $[2M + H]^+$, 1183.06 $[3M + H]^+$. IR (KBr) ν (cm^{-1}): 3394, 3278 (NH), 1605 (C═N), 1551, 1508, 1491 (thioamide I + HNH, CC_{ar}), 867 (thioamide IV), 830 (CH_{oop}), 456, 441 (Ni—N), 355, 351 (Ni—S). ^{1}H NMR (300 MHz, DMSO-d_6) δ (ppm): 9.76 (s, 1H, H_{6a}), 7.57 (b s, 2H, $H_{1a} + H_{1b}$), 7.50 (d, $J = 9.2$ Hz, 2H, $H_8 + H_4$), 6.86 (d, $J = 9.2$ Hz, 2H, $H_9 + H_{11}$), 3.70 (s, 3H, H_{13}), 2.02 (s, 3H, H_6), 1.92 (s, 3H, H_5). ^{13}C NMR (75 MHz, DMSO-d_6) δ (ppm): 179.5, 172.6 (C_1, C_4), 158.9 (C_{10}), 155.4, 154.7 (C_2, C_3), 134.2 (C_7), 121.6 ($C_9 + C_{11}$), 114.2 ($C_8 + C_{12}$), 55.6 (C_{13}), 14.9, 14.3 (C_5, C_6). UV–vis (DMSO) λ_{max} nm (L mol^{-1} cm^{-1}): 270 (34,490), 440 (14,480), 677 (670).

2.2.6 | $[ZnL^3(OH_2)]$ (**6**)

Brown, 130 mg, 93%. Anal. calcd. for $ZnC_{13}H_{18}N_6S_2O_2$ (MW 419.83) (%): C, 37.19; H, 4.32; N, 20.02; S, 15.27. Found (%): C, 37.34; H, 4.14; N, 19.85; S, 15.07. ESI-MS m/z: 401.02 $[ZnL^2 + H]^+$, 801.03 $[Zn_2(L^2)_2 + H]^+$, 1201.04 $[Zn_3(L^2)_3 + H]^+$. IR (KBr) ν (cm^{-1}): 3489, 3310, 3275, 3182, 3121 (OH + NH), 1628, 1608 (HOH + C═N), 1542, 1508, 1486, 1450 (thioamide I + HNH + CC_{ar}), 857 (thioamide IV), 825 (CH_{oop}), 490, 471 (Zn—N), 383, 375 (Zn—S). ^{1}H NMR (300 MHz, DMSO-d_6) δ (ppm): 9.20 (s, 1H, H_{6a}), 7.72 (d, $J = 9.0$ Hz, 2H, $H_8 + H_{12}$), 7.02 (s, 2H, $H_{1a} + H_{1b}$), 6.84 (d, $J = 9.0$ Hz, 2H, $H_9 + H_{11}$), 3.71 (s, 3H, H_{13}), 2.28 (s, 3H, H_6), 2.21 (s, 3H, H_5). ^{13}C NMR (75 MHz, DMSO-d_6) δ (ppm): 179.0, 172.9 (C_1, C_4), 154.7 (C_3), 154.5, 148.5 (C_2, C_3), 135.1 (C_7), 121.8 ($C_9 + C_{11}$), 1114.0 ($C_8 + C_{12}$), 15.1, 14.4 (C_5, C_6). UV–vis (DMSO) λ_{max} nm (L mol^{-1} cm^{-1}): 260 (14,460), 330 (12,590), 450 (16,950).

2.3 | Computational studies

All calculations were carried out using the GAMESS program.[32] The computational models were built by considering the single-crystal X-ray diffraction data and the structures optimized by molecular mechanics calculations, in particular Universal Force Field (UFF) using the Avogadro 1.2.0 program,[33] for the complexes without it. The aforementioned models were fully optimized at the scalar relativistic DFT level using the LANL2DZ basis set. The methodology was validated based on structural determinations between crystallographic and experimental section data.

2.4 | Testing of the photocatalytic activity for the degradation of MO

The photocatalytic activity of the six complexes for the degradation of MO was evaluated by preparing a suspension of 8 mg of the complex in 8 mL of a 10^{-5}-M solution of MO in water in a sealed vial. The mixture was stirred while irradiated with a high-pressure mercury vapor lamp (250 W, HPL-N Philips, Amsterdam, the Netherlands). Aliquots of 1 mL were taken with a syringe after different irradiation times, and their absorption spectra were recorded on the spectrophotometer. The concentration of MO was calculated by analyzing the changes in the absorbance at 465 nm. In cases where the MO signal overlapped with other signals, the spectra were deconvoluted to unambiguously assign the intensity of the MO absorption maximum to the MO concentration. To prevent a higher decrease in the value of MO concentration, two side effects were considered when the data were analyzed: the self-degradation of MO only with UV–vis irradiation and/or its degradation in the absence of light (non-photocatalytic degradation). Therefore, two additional experiments were carried out: A solution of MO without any complex was irradiated under the same experimental conditions, and no degradation of MO was indeed produced. Moreover, suspensions with MO and the different complexes were prepared as described above, but they were kept in the dark, resulting in no changes in the MO concentration, discarding non-photocatalytic degradation in all cases. The experiments were repeated three times, observing, in all cases, a statistical uncertainty below 1%.

2.5 | Testing of the photocatalytic activity for water splitting

The photocatalytic activity of the nickel complexes was measured by preparing a suspension of 11 mg of the complex in a mixture of 5.5 mL of water and 5.5 mL of methanol in a sealed vial. After flowing the reaction mixture with N_2 for 10 min in dark conditions, it was then irradiated for 30 min by a 300-W Xe lamp positioned in front of the sealed vial. Gas samples of 1 mL were taken from the headspace and injected immediately into a gas chromatograph (Agilent GC 8860) equipped with HP-PLOT-Q and HP-PLOT-Mole sieve 5 Å columns (0.53/0.32 mm I.D. 30 m) and a thermal conductivity detector (TCD) or a flame ionization detector (FID). The reported results are the average of three independent experiments, and control experiments were performed under the same conditions but in the absence of the catalyst.

2.6 | Crystallographic data and structure determination

Complexes **3**, **5**, and **6** were recrystallized from DMSO solutions. Crystallographic data were collected on a Bruker Kappa Apex II diffractometer equipped with an Apex II charged-coupled device (CCD) area detector using a graphite monochromator (Mo k_α radiation, $\lambda = 0.71073$ Å). CCDC numbers 2286636–2286638 contain the supplementary crystallographic data for complexes **3**, **5**, and **6**, respectively. These data can be obtained free of charge via http://www.ccdc.cam.ac.uk/conts/retrieving.html, or from the Cambridge Crystallographic Data Centre, 12 Union Road, Cambridge CB2 1EZ, UK; fax: (+44) 1223-336-033; or e-mail: deposit@ccdc.cam.ac.uk.

3 | RESULTS AND DISCUSSION

Three new hybrid bis(thiosemicarbazone) ligands have been synthesized following an analogous procedure to the one previously reported by the group for related ligands (Scheme 1).[31] This implies two successive condensation reactions, which must be carefully controlled to avoid obtaining undesired by-products. The key reaction is the synthesis of the monoketone obtained by the condensation of thiosemicarbazide with 2,3-butanedione, as the formation of the symmetrical bis(thiosemicarbazone) or the 1,2,4-triazine-3-thione—by cyclization of the monoketone—can happen, preventing the formation of the unsymmetrical ligand. The formation of this undesired product can be avoided by using an excess of dicarbonyl and using water as a solvent, in which the monoketone is completely unsoluble. The dissymmetric ligands are synthesized in good yield after the subsequent condensation of the corresponding 4-R-thiosemicarbazide (R = naphthyl, 4-methoxyphenyl, or 4-chlorophenyl).

The ligands were reacted with nickel(II) and zinc(II) nitrate hexahydrate, leading to the formation of six coordination compounds (Scheme 1). In the reactions with Zn(II), lithium hydroxide monohydrate was added to assure ligand deprotonation, whereas in the case of nickel(II), the ligands deprotonate even in the absence of base.

The elemental analysis agrees with a 1:1 ligand-to-metal stoichiometry and discards the presence of nitrate, suggesting that the ligands behave as dianionic donors. In addition, the zinc(II) complexes support the presence of a water molecule.

The mass spectra of the three ligands (Figures S1–S3) show the peak corresponding to $[M + H]^+$ as the base peak. The spectra of the six complexes (Figures S4–S9) confirm their formation and exhibit the fragment $[ML + H]^+$ as the most intense peak, but peaks corresponding to $[M_2L_2 + H]^+$ and in the zinc complexes also to $[M_3L_3 + H]^+$ and even $[M_4L_4 + H]^+$ species are also observed, but with much lower intensity. These peaks containing more than one metal are probably due to the formation of very strong hydrogen bonds rather than covalent polynuclear species, as confirmed by the single-crystal X-ray diffraction (see below).

3.1 | Crystal structures

The crystal structure of complexes **3**, **5**, and **6** was solved by the single-crystal X-ray diffraction. The refinement

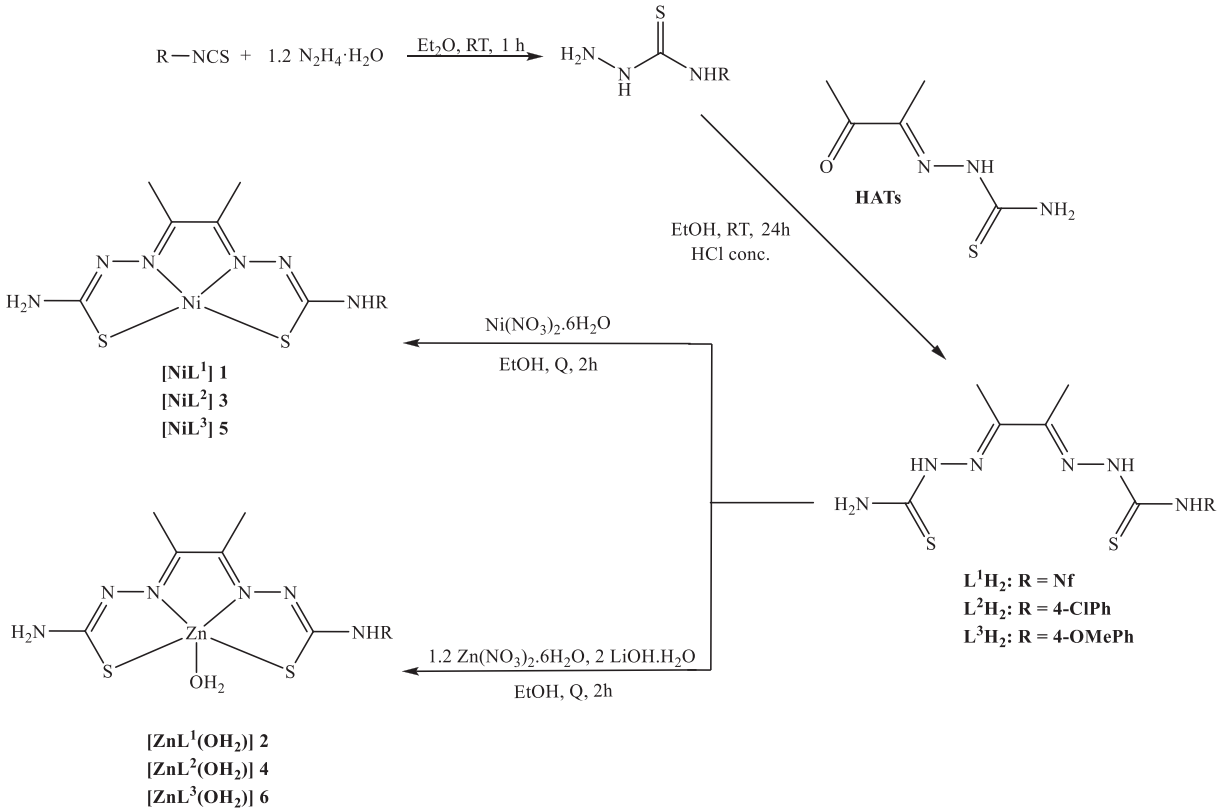

SCHEME 1 Synthesis of the organic molecules and the coordination compounds.

and crystallographic data are collected in Table 1, and selected bond distances are in Table 2.

The three complexes are monomeric species in which the ligands are doubly deprotonated, leading to some degree of electronic delocalization over the ligand backbone. The N_2S_2 coordination mode produces three five-membered chelate rings, which provide great stability to the complexes.

Complexes **3** and **5** crystallize with two DMSO molecules linked by hydrogen bonds to the NH_2 and NH groups, leading to the formation of dimers. The structures of the complexes are shown in Figure 1 (complex **3**) and Figure 2 (complex **5**). In both complexes, the nickel is in a square planar environment with $\tau_4 = 0.14$ for both complexes ($\tau_4 = 1$ for tetrahedral and 0 for square planar),[34] and the ligand cores, including the aromatic rings, are virtually planar.

The asymmetric unit of complex **6** contains one [ZnL^3(DMSO)] unit (Figure 3) and two crystallization DMSO molecules. The DMSO has replaced the water molecule that was proposed to be coordinated before its recrystallization, and it is coordinated through the

TABLE 1 Crystallographic and refinement data for complexes [NiL^2]·2DMSO, [NiL^3]·2DMSO, and [Zn(DMSO)L^3]·2DMSO.

	[NiL^2]·2DMSO	[NiL^3]·2DMSO	[Zn(DMSO)L^3]·2DMSO
Formula	$NiC_{16}H_{25}ClN_6O_2S_4$	$NiC_{17}H_{28}N_6O_3S_4$	$ZnC_{19}H_{34}N_6O_4S_5$
M	555.82	551.40	636.19
Temperature (K)	200(2)	200(2)	289(2)
Crystal system	Monoclinic	Monoclinic	Monoclinic
Space group	P 21/c	P 21/c	P 21/n
a (Å)	19.7575(11)	12.4661(6)	12.6976(5)
b (Å)	12.0666(6)	11.3716(6)	13.3474(5)
c (Å)	10.2679(6)	35.143(2)	17.4470(6)
α (°)	90	90	90
β (°)	98.752(3)	99.512(2)	94.774(2)
γ (°)	90	90	90
U ($Å^3$)	2419.4(2)	4913.4(4)	2946.66(19)
Z	4	8	4
D_c (Mgm^{-3})	1.526	1.491	1.223
Absorption coefficient (mm^{-1})	1.283	1.160	1.021
F(000)	1152	1202	1328
Goodness of fit on F^2	1.424	1.009	0.878
Reflections collected	15,907	51,831	61,012
Independent reflections	24,565 [R(int) = 0.0713]	9086 [R(int) = 0.1254]	6087 [R(int) = 0.0545]
Final R1 and wR2 [$I > 2\sigma(I)$]	0.0769, 0.2095	0.0624, 0.1445	0.0580, 0.1792
R indices (all data)	R1 = 0.1295, wR2 = 0.2414	R1 = 0.1552, wR2 = 0.2012	R1 = 0.0813, wR2 = 0.21618
Residual electron density (min, max) ($eÅ^{-3}$)	−1.330, 1.332	−0.585, 1.017	−0.956, 1.329

Abbreviation: DMSO, dimethyl sulfoxide.

TABLE 2 Selected bond distances in complexes [NiL^2]·2DMSO, [NiL^3]·2DMSO, and [Zn(DMSO)L^3]·2DMSO.

	[NiL^2]·2DMSO	[NiL^3]·2DMSO	[Zn(DMSO)L^3]·2DMSO
M(1)—N(3)	1.857(6)	1.859(5)	2.117(3)
M(1)—N(4)	1.837(6)	1.844(5)	2.092(3)
M(1)—S(1)	2.150(2)	2.142(2)	2.3510(11)
M(1)—S(2)	2.148(2)	2.142(2)	2.3476(11)
Zn(1)—O(2)	-	-	2.058(3)

Abbreviation: DMSO, dimethyl sulfoxide.

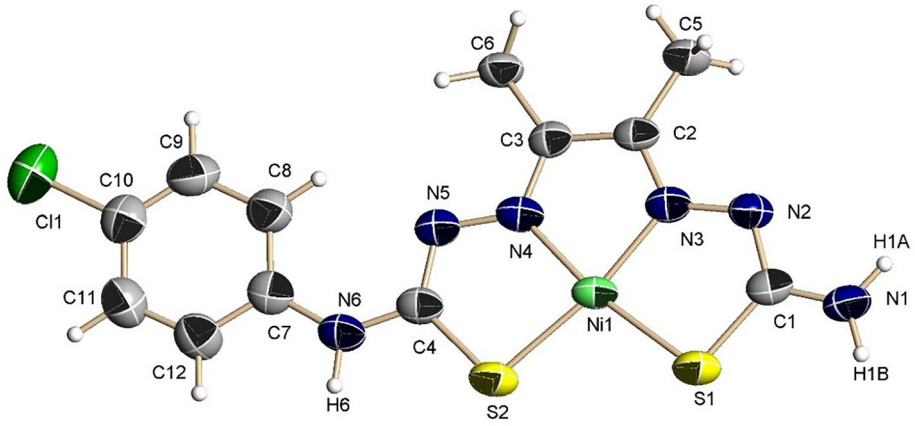

FIGURE 1 Molecular structure of $[NiL^2]\cdot 2DMSO$. Thermal ellipsoids at a 50% probability level. The two dimethyl sulfoxide (DMSO) molecules are omitted for clarity.

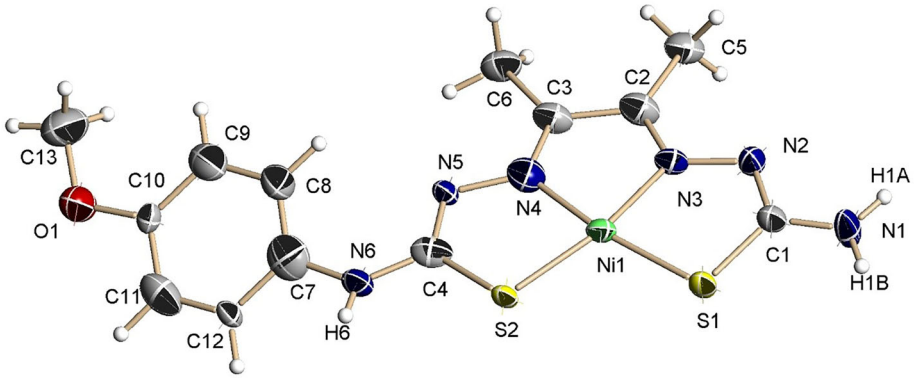

FIGURE 2 Molecular structure of $[NiL^3]\cdot 2DMSO$. Thermal ellipsoids at a 50% probability level. The two dimethyl sulfoxide (DMSO) molecules are omitted for clarity.

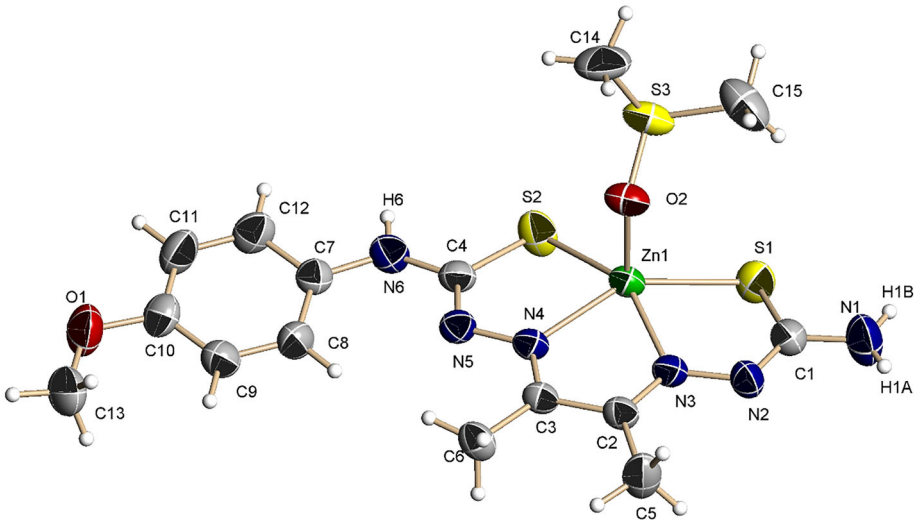

FIGURE 3 Molecular structure of $[Zn(DMSO)L^3]\cdot 2DMSO$. Thermal ellipsoids at a 50% probability level. The two dimethyl sulfoxide (DMSO) molecules of crystallization are omitted for clarity.

oxygen atom. The metal is in a square pyramidal geometry ($\tau_5 = 0.05$; $\tau_5 = 1$ for trigonal bipyramid and $\tau_5 = 0$ for square-base pyramid),[35] with the DMSO molecule occupying the apical position. The ligand core is deviated from planarity, and the metal is 0.413 Å above the least squares plane. The aromatic ring is now canted and forms an angle of 13.34° with the ligand backbone. The hydrogen bonds are the same as for complexes **3** and **5** and involve the crystallization of DMSO molecules, the NH_2 and NH groups, leading to the formation of dimers.

3.2 | IR spectroscopy

The IR spectra of HATs exhibit a strong peak at 1685 cm^{-1}, corresponding to the C═O group that disappears after the reaction with the 4-substituted-thiosemicarbazone. This, together with the presence of more signals attributable to ν(N—H) and new bands corresponding to $\nu(C—H)_{ar}$, $\nu(C—C)_{ar}$, and $\delta(C—H)_{oop}$, supports the formation of the dissymmetric ligands (Figures S10–S12). The absence of a band around

2600 cm^{-1} discards the presence of the thiol tautomeric form and agrees with the imine–thione form of the ligands. In the spectra of the complexes (Figures S13–S18), it can be clearly observed that there is a decrease in the number of ν(N—H) bands, suggesting ligand deprotonation, which is supported by the absence of a strong band at 1385 cm^{-1} corresponding to the nitrate ion. In addition, the bands corresponding to ν(C═N) and ν(C═S) are shifted with respect to the free ligands, showing the coordination of both groups with the metals. Moreover, in the zinc complexes, bands corresponding to ν(O—H) and (H—O—H) of the coordinated water molecule are also observed.

3.3 | NMR spectroscopy

The ^{1}H NMR spectra of the organic compounds (Figures S19–S21) show the signals with the multiplicities and the integrals expected for their structures. In the spectra of the monoketone, the chemical shifts of the two methyl groups are quite different because one is bonded to a C═O group (2.40 ppm) whereas the other is attached to a C═N group (1.95 ppm), but in the dissymmetric ligands, their chemical shifts are almost identical and appear around 2.26 ppm. The aromatic protons in $L^{1}H_2$ appear as four multiplets between 8.02 and 7.52 ppm, whereas in $L^{2}H_2$ and $L^{3}H_2$, they appear as two doublets at 7.62 and 7.43 and 7.41 and 6.94, respectively, which indicates that there is more electronic density in the aromatic ring with the OCH_3 substituent, due to the mesomeric effect, positive for the OMe group and negative for chloride. In the spectrum of $L^{3}H_2$, a signal at 3.77 ppm, corresponding to the methoxy groups, can also be observed. In all the ligands, the two protons of the NH_2 group are diastereotopic. In the spectra of the coordination compounds (Figures S22–S27), the absence of the acidic protons H_2 and H_{5a} can be clearly observed, confirming the ligand double deprotonation. The rest of the signals are, in general, upfield shifted with respect to the free ligands as a consequence of the bond with the metal ion. The two protons of the NH_2 group are now equivalent, and in the nickel complexes, they appear as a broad singlet and as a sharp one in the zinc derivatives. In complexes **2**, **4**, and **6**, the signal of the water molecule coordinated to zinc cannot be observed, probably because it is obscured by the strong signal due to the water present in the DMSO-d_6.

In the ^{13}C NMR spectra of the three ligands (Figures S28–S30), two signals correspond to the thione groups and two to the imine groups, confirming their dissymmetric structures. The signals of the TSC branch appear at a lower field than the ones corresponding to 1-naphthyl, 4-chlorophenyl, and 4-methoxyphenyl TSCs. In addition, a signal for each of the carbons present in their structures can be clearly observed. After complexation (Figures S31–S36), the signals corresponding to the C═N groups are shifted with respect to the free ligand, especially in the nickel complexes, but this shift is much smaller for the signals assigned to the C═S groups. This small shift does not preclude S-coordination, and both imine and thione groups are coordinated to the metal, as confirmed by the X-ray diffraction, but the possibility of π-back bonding in the C═S groups results in a small variation in the electronic density on the carbon and therefore induces a small change in the chemical shift.

3.4 | Photocatalytic degradation of MO

The photocatalytic activity of the compounds was evaluated by monitoring the MO decomposition in an aqueous solution under UV–vis light irradiation. MO is a common synthetic anionic azo dye that is generally used as a coloring agent in the textile and leather industries, and it is also widely used in the printing, paper manufacturing, pharmaceutical, food processing, and research laboratories. It is harmful to the environment and biology, so it must be treated innocuously before it can be discharged.[36] Figures 4 and 5 show the photoactivity under UV–vis irradiation of the zinc and nickel complexes **1**–**6**, and, as observed, they effectively degrade the organic dye, although with some differences. As can be seen in Figure 4c, complex **5** produces the least MO degradation among the nickel complexes, which could be related to a partial dissolution of the complex in the reaction medium, which is observed by the appearance in the UV–vis spectra (Figures S37–S42) of a strong new band around 420 nm, even at time = 0. This partial solubilization of the complex in the medium is also observed for complexes **3** and **6**, but to a lesser extent and following the opposite trend, that is, increasing with time, although it probably also reduces the photoactivity. Nevertheless, complex **3** is the most photoactive for MO degradation. These results show that the photoactivity of these complexes is much higher than for other nickel(II) complexes with bis(thiosemicarbazone) ligands reported by our group, which only degrade 5% of MO in 24 h,[30] confirming the decisive role that the ligands play in the photocatalytic activity. Regarding the zinc complexes (Figure 5), we observe that in this case, as with the nickel compounds, the complex bearing the 4-chlorophenyl substituent (complex **4**) is the most photoactive, degrading 50% of MO in approximately 20 h. However, unlike the nickel complexes, a limiting concentration of MO at which the degradation rate is drastically reduced (20% of the initial concentration) is reached at 48 h. The same happens for

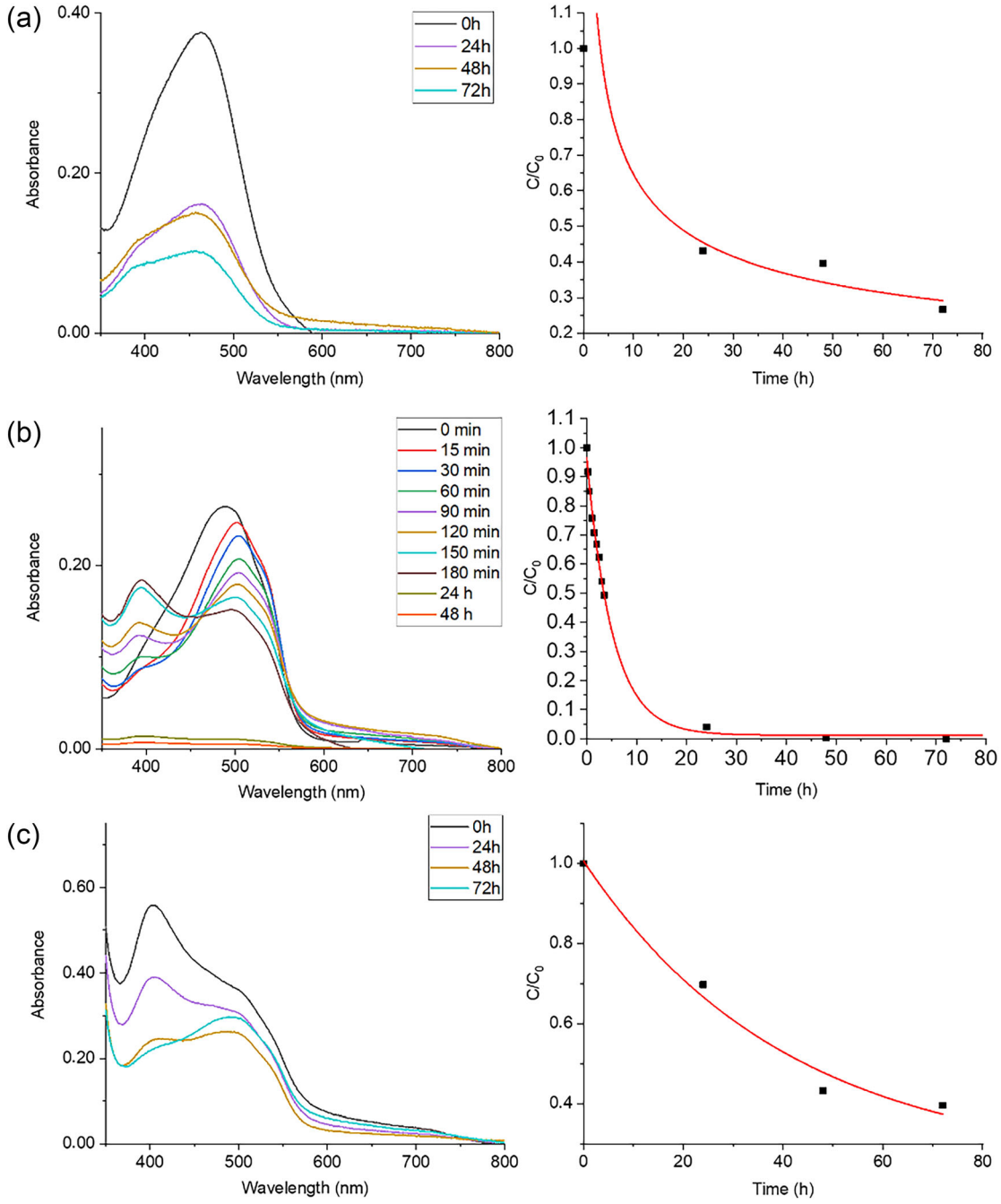

FIGURE 4 UV–vis spectra and evolution of the methyl orange concentration with the reaction time for the nickel complexes: (a) complex **1**, (b) complex **3**, and (c) complex **5**.

complex **6** (ligand with a 4-methoxyphenyl substituent), but this behavior is not observed for complex **2** (naphthyl substituent), which has degraded 30% of MO in 144 h without reaching a plateau. A possible explanation for this phenomenon could be a passivation of the photocatalysis due to a reduced concentration of MO,[37] but in the case of complex **2**, this is not observed as, being a much slower reaction, the limiting concentration has not yet been reached.

If we look at the time in which the degradation of half of the initial concentration of MO is reached (Table 3), we can observe the following order of kinetic rates: complex **3** > complex **1** > complex **4** > complex **6** > complex **5** > complex **2**. Based on these results, some general tendencies can be observed: The complexes with the ligand bearing a 4-chlorophenyl substituent, complexes **3** and **4**, are the ones that present better photodegradation percentages of MO. In addition, the nickel complexes **1** and **3** show better photoefficiency, both for presenting faster degradation kinetics and for not presenting a limit concentration from which the photocatalysis slows down, as happens with the zinc complexes. In contrast, the nickel

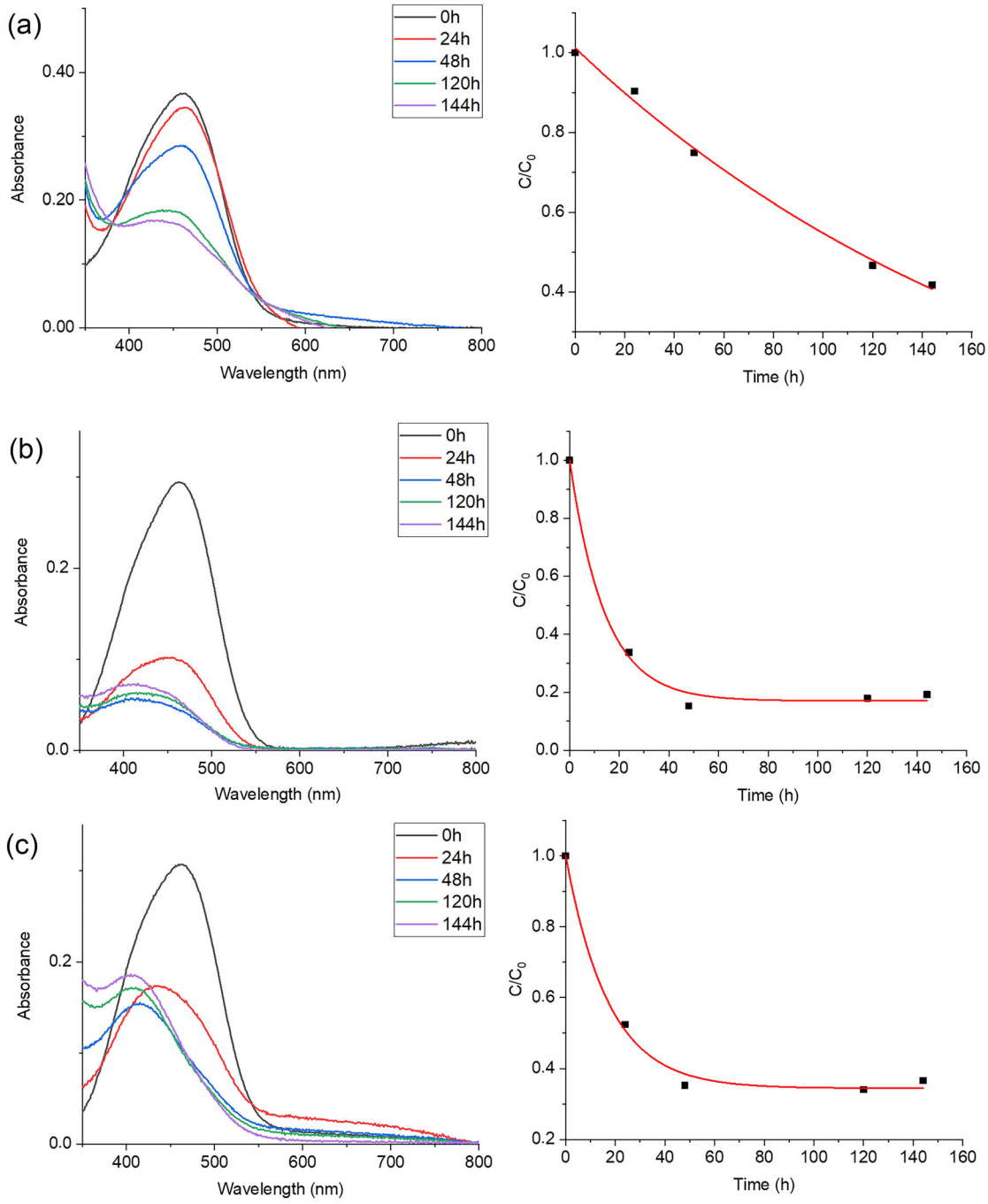

FIGURE 5 UV–vis spectra and evolution of the methyl orange concentration with the reaction time for the zinc complexes: (a) complex **2**, (b) complex **4**, and (c) complex **6**.

complex with 4-methoxyphenyl **5** is less efficient, which could be affected because its solubility in the medium affects its photoactivity.

3.5 | DFT calculations

In order to try to justify this observed trend, computational calculations were performed. The results obtained seem to coincide with the trend observed experimentally, showing that the complexes show a highest occupied molecular orbital (HOMO)–lowest unoccupied molecular orbital (LUMO) gap (Table 3 and Figure 6), varying in the following order: complex **5** > complex **3** > complex **1** > complex **4** > complex **6** > complex **2**. As can be seen, complex **3**, which shows the best degradation kinetics, has a HOMO–LUMO gap of 1.279 eV, and this difference gradually decreases until reaching 0.109 eV for complex

TABLE 3 Molecular orbital (MO) composition and energy values of the HOMO, LUMO, HOMO–LUMO (H–L) gaps, and the 50% degradation time of methyl orange for the systems. All the energies are reported in electron volts, and the time is in hours.

System	E_{HOMO}	MO composition	E_{LUMO}	MO composition	H–L gap	50% degradation time
1	−9.061	95% ligand 5% Ni	−8.354	100% ligand	0.707	15 h
2	−9.742	90% ligand 10% Zn	−9.633	50% ligand 50% Zn	0.109	120 h
3	−3.837	85% ligand 15% Ni	−2.558	50% ligand 50% Ni	1.279	4 h
4	−9.660	80% ligand 20% Zn	−9.007	50% ligand 50% Zn	0.653	18 h
5	−9.470	85% ligand 15% Ni	−3.864	100% ligand	5.606	40 h
6	−9.959	95% ligand 5% Zn	−9.442	50% ligand 50% Zn	0.517	24 h

Abbreviations: HOMO, highest occupied molecular orbital; LUMO, lowest unoccupied molecular orbital.

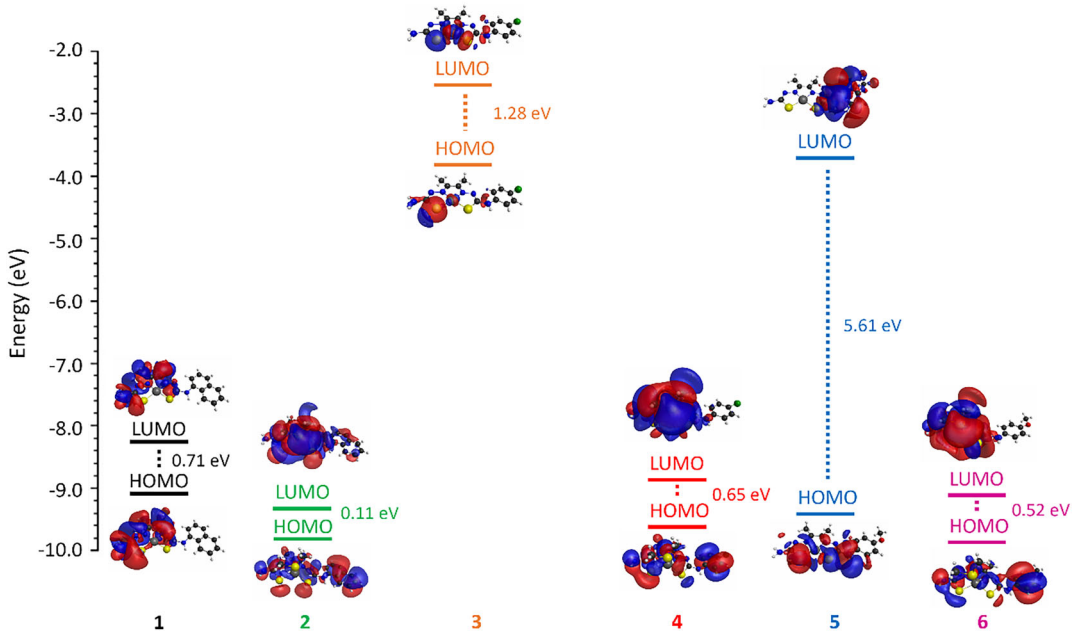

FIGURE 6 Energy diagram of the frontier molecular orbitals for the complexes **1**–**6**. The dashed colored lines represent the highest occupied molecular orbital (HOMO)–lowest unoccupied molecular orbital (LUMO) gap.

2, which shows the slowest degradation kinetics. This order coincides with the degradation kinetics observed experimentally, except for complex **5**, which shows an abnormally high HOMO–LUMO gap of 5.606 eV, which would justify why its degradation kinetics place it in the penultimate position. In addition, the HOMO and LUMO orbitals of complex **3**, which shows better photoactivity, have higher energy, which may also explain why the photoactivity is so different from the rest, taking approximately four times less time to degrade MO than the second most photoactive complex, complex **1**.

From all the results described above, it seems that an adequate energy of the HOMO and LUMO orbitals, together with their energy gap, is an important parameter for the photodegradation of MO to occur.

A plausible photodegradation mechanism of MO is that the TSC complex captures MO molecules onto its surface. According to this, the better photoactivity found for the nickel complexes could be due to their different geometry, which is a consequence of the metal preferences: Whereas nickel complexes are square planar, zinc derivatives present a square-base pyramid geometry,

making the metal center less accessible and causing a worse photocatalytic activity. Then, the excited electrons transit from the HOMO to LUMO orbitals, producing pairs of electrons and void spaces (h^+) under UV–vis light irradiation. Highly oxidative $^{\bullet}OH$ radicals are produced by the h^+ oxidation of H_2O or —OH and can photodegrade MO molecules. Additionally, h^+ can directly decompose molecules adsorbed on its surface. The photogenerated electrons in the LUMO are scavenged by O_2 to produce $^{\bullet}O_2^-$, which provides peroxide radical ($^{\bullet}OOH$) on protonation. $^{\bullet}O_2^-$ can also photodegrade the MO molecules. This mechanism is in agreement with one recently proposed for the degradation of methylene blue by a monothiosemicarbazone complex.[38]

3.6 | Photocatalytic water splitting

The catalytic activity of the nickel complexes in promoting water splitting under light irradiation was analyzed by measuring the amount of H_2 evolved in the reaction by gas chromatography. The preliminary results indicate that complex **3** does not photocatalyze the water splitting in the reaction conditions tested (11 mL of water/methanol 1:1, 11 mg of the complex, 30 min of irradiation), but in the case of complexes **1** and **5**, the production of H_2 was detected. In these conditions, complex **1** produces 2.61 μmol h^{-1} g^{-1}, while complex **5** produces 30.63 μmol h^{-1} g^{-1}. There are very few reports on the use of TSC complexes in this type of reaction, but usually, the photocatalysis is carried out in the presence of a photosensitizer such as nanorods and an additional sacrificial electron donor (SED) such as triethylamine or ascorbic acid.[39] These preliminary results show that our nickel complexes have the potential to be used in the design of efficient photocatalytic systems for water splitting, as even in the absence of a photosensitizer and only with methanol as SED, they evolve hydrogen in equivalent amounts to other reported symmetrical bis(thiosemicarbazone) complexes used together with tris(2-carboxyethyl)phosphine/ascorbic acid as SED and nitrogen-doped carbon dots as photosensitizers.[40] This apparent better performance of our complexes could be related to the asymmetry of the ligands.

4 | CONCLUSIONS

Three new dissymmetric bis(thiosemicarbazone) ligands have been synthesized with high purity and yield. By reaction with nickel(II) and zinc(II) nitrates, six new coordination compounds have been synthesized and fully characterized. In the nickel complexes, the metal is in a square planar coordination environment, while in the zinc derivatives, it has a square-base pyramid geometry.

Their photocatalytic activity for MO degradation was also evaluated. The results show that all the compounds photocatalyze this reaction. Within the nickel compounds, complex **3** exhibits the fastest kinetics, degrading 50% of the contaminant in 4 h and 100% in 24 h. The degradation by the zinc complexes is slower, and complexes **4** and **6** reach a plateau in 48 h, when complex **4** has degraded 80% of MO and complex **6** 65%. This plateau is not observed for complex **2**, probably because its kinetic rate is much slower and has not yet been reached.

DFT calculations were carried out to justify the results obtained and indicate a clear relationship between the HOMO–LUMO energy differences and the energy values, as the complex with the best photoefficiency has a HOMO–LUMO gap of 1.279 eV and the orbitals have the highest energies. Deviations from this gap and a significant decrease in the orbital energies induce a decrease in the MO degradation rate. Complex **5** presents an abnormally high band gap, which causes it to be the less efficient complex, which is probably also affected because its solubilization in the reaction media is interfering with the catalytic process.

Photocatalytic hydrogen production by water splitting, promoted by nickel complexes, was also tested. The results show that the complex can evolve molecular hydrogen even in the absence of a photosensitizer and an SED, but further experiments analyzing different parameters, such as the amount of the catalyst, the pH, the effect of the solvent ratio in the photocatalytic mixture, and the nature of the SED and the photosensitizer, should be done to set the characteristics of the most efficient photocatalytic system.

AUTHOR CONTRIBUTIONS

Rodrigo Burón: Investigation. **Daniel Jiménez-Gómez:** Resources. **David G. Calatayud:** Investigation; writing—review and editing. **Ana Iglesias-Juez:** Resources. **Fernando Fresno:** Resources. **M. Antonia Mendiola:** Writing—review and editing. **Elena López-Torres:** Conceptualization; supervision; writing—review and editing.

ACKNOWLEDGMENTS

The authors thank the Ministerio de Ciencia e Innovación (MICINN) (Project PID2019-104118RB-C21) for funding.

CONFLICT OF INTEREST STATEMENT

There are no conflicts of interest to declare.

DATA AVAILABILITY STATEMENT

All spectroscopic information and spectral data are available with the corresponding authors.

REFERENCES

[1] F. Z. Akika, K. Rouibah, M. Benamira, I. Avramova, *Inorg. Chem. Commun.* **2023**, *154*, 110878.
[2] A. Tkaczyk, K. Mitrowska, A. Posyniak, *Sci. Total Environ.* **2020**, *714*, 137222.
[3] K. Matsuyama, Y. Kawahara, A. Shoji, T. Kato, T. Okuyama, *J. Appl. Polym. Sci.* **2023**, *140*, e54347.
[4] A. K. Badawi, R. S. Salama, M. M. M. Mostafa, *RSC Adv.* **2023**, *13*, 19335.
[5] S. Ahmadipouya, S. A. Mousavi, A. Shokrgozar, D. V. Mousavi, *J. Environ. Chem. Eng.* **2022**, *10*, 107535.
[6] B. E. Barragán, C. Costa, M. C. Márquez, *Dyes Pigment.* **2007**, *75*, 73.
[7] V. K.-M. Au, S. Y. Kwan, M. N. Lai, K.-H. Low, *Chem. – Eur. J.* **2021**, *27*, 9174.
[8] M. Y. Rizala, R. Saleha, A. Taufik, *J. Environ. Chem. Eng.* **2020**, *8*, 103610.
[9] R. Comparelli, E. Fanizza, M. L. Curri, P. D. Cozzoli, G. Mascolo, R. Passino, A. Agostiano, *Appl. Catal. B-Environ.* **2005**, *55*, 81.
[10] S. S. F. Carvalho, A. C. C. Rodrigues, J. F. Lima, N. M. F. Carvalho, *Inorg. Chim. Acta* **2020**, *512*, 119924.
[11] S. J. Jennifer, A. K. Jana, *Cryst. Growth Des.* **2017**, *17*, 5318.
[12] K. Ghosh, K. Harms, A. Franconetti, A. Frontera, S. Chattopadhyay, *J. Organomet. Chem.* **2019**, *883*, 52.
[13] B. Shakya, P. N. Yadav, *Mini-Rev. Med. Chem.* **2020**, *20*, 638.
[14] J. Devi, M. Yadav, D. K. Jindal, D. Kumar, Y. Poornachandra, *Appl. Organometal. Chem.* **2019**, *33*, e5154.
[15] K. Bajaj, R. M. Buchanan, C. A. Grapperhaus, *J. Inorg. Biochem.* **2021**, *225*, 111620.
[16] G. L. Parrilha, R. G. dos Santos, H. Beraldo, *Coord. Chem. Rev.* **2022**, *458*, 214418.
[17] K. Murugan, S. Vijayapritha, P. Viswanathamurthi, K. Saravanan, P. Vijayan, S. O. Ojwach, *Inorg. Chim. Acta* **2020**, *512*, 119864.
[18] A. Ravindran, D. Sindhuja, N. Bhuvanesh, R. Karvembu, *Eur. J. Inorg. Chem.* **2022**, *2022*, e202200181.
[19] T. S. Lobana, R. Sharma, G. Bawa, S. Khanna, *Coord. Chem. Rev.* **2009**, *253*, 977.
[20] J. P. Holland, F. I. Aigbirhio, H. M. Betts, P. D. Bonnitcha, P. Burke, M. Christlieb, G. C. Churchill, A. R. Cowley, J. R. Dilworth, P. S. Donnelly, J. Green, J. M. Peach, S. R. Vasudevan, J. E. Warren, *Inorg. Chem.* **2007**, *46*, 465.
[21] M. Christlieb, J. R. Dilworth, *Chem. – Eur. J.* **2006**, *12*, 6194.
[22] D. G. Calatayud, E. López-Torres, M. A. Mendiola, *Eur. J. Inorg. Chem.* **2013**, *2013*, 80.
[23] D. G. Calatayud, E. López-Torres, J. R. Dilworth, M. A. Mendiola, *Inorg. Chim. Acta* **2012**, *381*, 150.
[24] D. G. Calatayud, E. López-Torres, M. A. Mendiola, *Polyhedron* **2013**, *54*, 39.
[25] E. Sesmero, D. G. Calatayud, J. Perles, E. López-Torres, M. A. Mendiola, *Eur. J. Inorg. Chem.* **2016**, *2016*, 1044.
[26] L. Alonso, R. Burón, E. López-Torres, M. A. Mendiola, *Crystals* **2022**, *12*, 310.
[27] M. G. Abd El-Nasser, S. A. Abdel-Latif, *Appl. Organometal. Chem.* **2023**, *37*, e6998.
[28] A. Z. Haddad, S. P. Cronin, M. S. Mashuta, R. M. Buchanan, C. A. Grapperhaus, *Inorg. Chem.* **2017**, *56*, 11254.
[29] T. Straistari, R. Hardré, J. Fize, S. Shova, M. Giorgi, M. Réglier, V. Artero, M. Orio, *Chem. – Eur. J.* **2018**, *24*, 8779.
[30] C. González-García, C. García-Pascual, R. Burón, D. G. Calatayud, J. Perles, M. A. Mendiola, E. López-Torres, *Polyhedron* **2022**, *223*, 115945.
[31] C. Huedo, F. Zani, M. A. Mendiola, S. Pradhan, C. Sinha, E. López-Torres, *Appl. Organometal. Chem.* **2019**, *33*, e-4700.
[32] G. M. J. Barca, C. Bertoni, L. Carrington, D. Datta, N. De Silva, J. E. Deustua, D. G. Fedorov, J. R. Gour, A. O. Gunina, E. Guidez, T. Harville, S. Irle, J. Ivanic, K. Kowalski, S. S. Leang, H. Li, W. Li, J. J. Lutz, I. Magoulas, J. Mato, V. Mironov, H. Nakata, B. Q. Pham, P. Piecuch, D. Poole, S. R. Pruitt, A. P. Rendell, L. B. Roskop, K. Ruedenberg, T. Sattasathuchana, M. W. Schmidt, J. Shen, L. Slipchenko, M. Sosonkina, V. Sundriyal, A. Tiwari, J. L. Gálvez Vallejo, B. Westheimer, M. Włoch, P. Xu, F. Zahariev, M. S. Gordon, *J. Chem. Phys.* **2020**, *152*, 154102.
[33] M. D. Hanwell, D. E. Curtis, D. C. Lonie, T. Vandermeersch, E. Zurek, G. R. Hutchison, *Aust. J. Chem.* **2012**, *4*, 17.
[34] L. Yang, D. R. Powell, R. F. Houser, *Dalton Trans.* **2007**, 955.
[35] A. W. Addison, T. N. Rao, J. Reedijk, J. van Rijn, G. C. Verschoor, *J. Chem. Soc., Dalton Trans.* **1984**.
[36] L. Wu, X. Liu, G. Lv, R. Zhu, L. Tian, M. Liu, Y. Li, W. Rao, T. Liu, L. Liao, *Sci. Rep.* **2021**, *11*, 10640.
[37] S. Zhu, D. Wang, *Adv. Energy Mater.* **2017**, *7*, 1700841.
[38] A. Lathe, K. Palanisamy, M. Prakash, A. M. Palve, *Inorg. Chem. Commun.* **2023**, *155*, 111064.
[39] W.-X. Jiang, Z.-L. Xie, S.-Z. Zhan, *Inorg. Chem. Commun.* **2019**, *102*, 5.
[40] K. Ladomenou, M. Papadakis, G. Landrou, M. Giorgi, C. Drivas, S. Kennou, R. Hardré, J. Massin, A. G. Coutsolelos, M. Orio, *Eur. J. Inorg. Chem.* **2021**, *2021*, 3097.

SUPPORTING INFORMATION

Additional supporting information can be found online in the Supporting Information section at the end of this article.

How to cite this article: R. Burón, D. Jiménez-Gómez, D. G. Calatayud, A. Iglesias-Juez, F. Fresno, M. A. Mendiola, E. López-Torres, *Appl Organomet Chem* **2024**, e7408. https://doi.org/10.1002/aoc.7408